https://dx.doi.org/10.1016/j.renene.2023.119426

Transparent wood with heat shielding and high fire safety properties for energy saving applications

Xin Hu[a,b 1], Yingbo Zhang[c 1], Wei Cai[a,b], Yang Ming[a,b], Rujun Yu[a,b], Hongyu, Yang[d], Nuruzzaman Noor[a, b]*, Bin Fei [a,b]*

a Materials Synthesis and Processing Lab, School of Fashion and Textiles, The Hong Kong Polytechnic University, Hung Hom, Kowloon, Hong Kong SAR, 999077, China.

b Research Centre for Resources Engineering towards Carbon Neutrality, The Hong Kong Polytechnic University, Hung Hom, Kowloon, Hong Kong SAR, 999077, China.

c Department of Building Environment and Energy Engineering, The Hong Kong Polytechnic University, Hung Hom, Kowloon, Hong Kong SAR, 999077, China

d College of Materials Science and Engineering, Chongqing University, Shazhengjie 174, Shapingba, Chongqing, 400030, China.

Abstract

Improving the energy efficiency of buildings is critical to achieving net-zero and addressing the global energy and climate crises. By adopting simple spin-coating, a solar-blocking coating ($Cs_{0.33}WO_3$) was prepared on transparent wood (TW). Meanwhile, a liquid and transparent flame retardant (BPDP) was employed to enhance its fire safety. The chemical composition, physical morphology, the thermal stability, and the fire safety of the resulting heat-shielding TW were analyzed using FTIR, XRD, SEM, TGA, and Cone, respectively. Field tests and simulations were conducted to evaluate the solar-blocking capacity and energy-saving potential of the heat-shielding. The char yield (CY) of heat-shielding TW was increased from 7.3% to 17.1% due to the catalytic carbonization effect of BPDP and inorganic coating. The heat-shielding TW demonstrated significant solar-blocking capabilities, with a 46.63% reduction in solar transmission compared to the original TW. The interior surface temperature (Ts) of the heat-shielding TW model was 10.2°C lower than that of normal glass, indicating its remarkable heat shielding performance. Energy-saving simulations based on experimental findings revealed that such heat-shielding TW achieved energy savings of 9.6%, 7.7%, and 6.2% in Hong Kong, Shanghai, and Singapore, respectively, when compared to traditional glazing glass. Overall, the prepared heat-shielding TW shows promise as a novel candidate for window applications, offering improved energy efficiency.

Keywords: Transparent wood, Heat-shielding, flame retardant, energy saving, sustainable materials.

Introduction

Buildings account for approximately 40% of global energy consumption. Among the various components of modern buildings, windows are particularly energy-inefficient, contributing to approximately 60% of total energy loss due to their inadequate thermal management capabilities [1, 2]. The most commonly used glazing material (i.e., glass) are suffering from a high thermal conductivity (~1 $W \cdot m^{-1} \cdot K^{-1}$), brittleness, and an energy-intensive production strategy. The glass manufacturing industry alone emits more than 60 million tons of CO_2 annually[3]. Meanwhile, the inevitable reflecting and glare effect of glass also lead to visual discomfort, lower working efficiency, poor emotional well-being, and even occasional accidents[4]. Consequently, there is a pressing need to explore glazing materials that offer improved energy efficiency, enhanced visual comfort, and sustainable manufacturing processes, while meeting minimum commercial safety and performance standards, to help achieve the goal of a carbon-neutral society, aligned with global initiatives for net-zero emissions by 2050[5-7].

Given the ease of processing, broad availability, low thermal conductivity and excellent mechanical performance, wood has been widely used throughout history for a range of structural and aesthetic applications. Recently, a novel wood product – transparent wood (TW) – has attracted wide attentions due to its high transmittance, sustainability, and low thermal conductivity [8-10], making it a promising material for window (among many other) applications. The preparation of TW commonly involves a discoloration process, specifically delignification or lignin-modification of a standard wood substrate, succeeded by polymer impregnation or a compression process. While the initial TW substrates have demonstrated potential as promising candidate for a wide range of applications, they have not yet attained the requisite properties to meet the demands of specialized functionalities in e.g., flame retardant applications. Despite outperforming traditional glasses in many aspects, TW faces challenges regarding fire safety, similar to those faced by established timber-based products[11]. Both the wood scaffold and impregnated polymers are highly flammable[12, 13], necessitating the consideration of fire safety before practical applications of TW. The organophosphate, tert-Butylphenyl Diphenyl Phosphate (BPDP), is a commercially available commonly used flame retardant (FR). It acts via a char formation mechanism, to physically protect the bulk material from further decomposition, and prevent any further flame spread while also minimizing smoke production[14]. Moreover, the liquid and transparent nature of BPDP provides chances for creating TW without unacceptable decreases in the optical properties.

Meanwhile, TW with various functionalities have also been developed [15], including heat shielding TW [16-18]. For example, Yu et al. prepared TW with NIR shielding by impregnating a cesium tungsten oxide (Cs_xWO_3) into the wood scaffold [16]. Cs_xWO_3 is a dark blue powder with excellent solar shielding additive that has potential

applications in smart windows, as it possesses high near-IR absorbency and reflectivity, while also retaining excellent visible light transparency. However, most of heat-shielding TW reported to-date were prepared by pre-functionalization, i.e., incorporated into the mixture with the refractive index (RI) matched polymers during the impregnation stage of TW formation. This approach requires a significant number of functional components, with only a small portion being integrated into the wood scaffold while the majority is wasted; it is an inefficient process that yields poorer TW substrate performance. Therefore, post-functionalization, referring to surface engineering and coating, might be promising way to achieve more effective heat-shielding functionality, with less functional components and less waste.

In this study, TW was prepared by lignin modification, followed by epoxy impregnation. TW with high luminous transmittance and remarkable near infrared (NIR) shielding ability was prepared by introducing a layer of $Cs_{0.33}WO_3$ onto its surface (FRTW@CWO_x). The physical morphology, chemical structure, fire performance, energy-saving potential, and spectra of FRTW@CWO_x were investigated. The FRTW@$CWO_{0.75}$ exhibited a luminous transmittance of 64.50%, making it ideal for window applications, while allowing only 11.04% of solar NIR irradiation to pass through. Field tests confirmed that FRTW@$CWO_{0.75}$ effectively reduced indoor temperatures by 10.2°C compared to conventional glass. Furthermore, energy simulations indicated that FRTW@$CWO_{0.75}$ could achieve energy savings of 9.6%, 7.7%, and 6.2% in annual heating and cooling consumption for Hong Kong, Shanghai, and Singapore, respectively. Meanwhile, the flame retardancy of TW was improved by introducing a commercially available liquid flame retardant (BPDP), which results in a reduction of 27.7 % in HRR compared to original TW. In addition, the intrinsic near-IR heat absorbing properties of $Cs_{0.33}WO_3$ were hypothesized to enhance the FR properties of the BPDP. With the combination of $Cs_{0.33}WO_3$ coating and BPDP, the char yield (CY) of heat-shielding TW was increased from 7.3% to 17.1%. The impressive heat-shielding capabilities, coupled with its fire safety position FRTW@$CWO_{0.75}$ as a highly promising option for energy-efficient windows.

Experiment

Materials and chemicals

Sodium silicate, sodium hydroxide, magnesium sulfate, diethylenetriaminepentaacetic acid, and hydrogen peroxide (30wt%) were provided by Macklin. Balsa wood (longitudinal) was supplied by Zhuhai DeChi Co., Ltd. Aero-Marine epoxy resin (#300 and #21) was used for polymer impregnating. Polyvinylpyrrolidone (PVP, Mw=58000, Acros Organic) were used to prepared coating solution. A commercially available liquid flame retardant (BPDP, Tert-Butylphenyl Diphenyl Phosphate, Fig. S1) was provided by Yarui chemical Co., Ltd. $Cs_{0.33}WO_3$ was purchased from Shanghai Yingcheng New Materials Co., Ltd. All chemicals were used without further purification and deionised (DI) water (18 MΩ) used, in all cases.

Preparation of flame-retardant TW substrates

The balsa wood was cut into 30 mm × 30 mm and 100 mm × 100 mm (For field test) slices with the thickness of 1.5 mm. The samples for cone calorimeter (cone) test were in the size of 10 cm × 10 cm ×3 mm. The preparation of TW follows previous reports with few modifications[19]. The lignin modification solution (DI water as solvent) was prepared by mixing following chemicals: sodium silicate (3.0 wt%), sodium hydroxide (3.0 wt%), magnesium sulfate (0.1 wt%), and diethylenetriaminepentaacetic acid (0.1 wt%), hydrogen peroxide (8.0 wt%). The balsa strips were immersed in the prepared solution and maintained at 70 ^{o}C for around 2 hours. Then the white wood strips were washed several times with DI water before being stored in ethanol for further use. Aero-Marine epoxy resin (#300 and #21) was used for polymer impregnation. The Epoxy resin #300 and curing agent #21 were mixed at a ratio of 2:1, while the ratio of BPDP to total epoxy weight was set to 10%. Lignin-modified wood strips were submerged in the epoxy precursor in a petri dish. Then, a vacuum of 0.1 atm was applied to the mixture for 15 mins, allowing the infiltration of epoxy in to the wood scaffold. The vacuum was repeated three times to ensure complete impregnation, after which, wood strips were sandwiched between two PET film sheets, and the samples cured at room temperature for 48 hours. Finally, the formed transparent wood (TW) was peeled off from the PET film. The resulting products were named as FRTW.

Preparation of heat-shielding TW

The prepared TW was used as the substrate for heat-shielding coating. The $Cs_{0.33}WO_3$ (0.25 g, 0.5 g and 0.75 g) and 0.5 g of PVP were dispersed in 10 ml ethanol solution with stirring. Then, the mixture was sonicated in the ultrasonic bath for 30 mins to obtain uniform solution. Before the coating process, TW substrates were washed with ethanol in ultrasonic bath for 2 mins. Finally, $Cs_{0.33}WO_3$ was spin-coated on the TW

substrate with the spinning speed of 1000 rpm using 500 μL of the coating solution. The resulting products were named as FRTW@$CWO_{0.25}$, FRTW@$CWO_{0.50}$ FRTW and FRTW@$CWO_{0.75}$.

Characterization

The morphologies of the samples were observed by Field Emission Scanning Electron Microscope (SEM, Tescan MAIA3). The transmittance spectra of samples across 200 nm to 2400 nm were collected by PERKIN ELMER UV-Vis-NIR Spectrometer with a 150 mm of integrating sphere. The transmittance T(λ) and reflectance R(λ) across 200-2400 nm were obtained from PERKIN ELMER UV-Vis-NIR Spectrometer with a 150 mm of integrating sphere. The T_{sol}, R_{sol}, and T_{lum} were determined by the following formula:

$$Tsol = \int_{200}^{2400} \varphi_{sol}(\lambda) \cdot T(\lambda)\, d\lambda / \int_{200}^{2400} \varphi_{sol}(\lambda)\, d\lambda \text{- - - - - - - - (1)}$$

$$Rsol = \int_{200}^{2400} \varphi_{sol}(\lambda) \cdot R(\lambda)\, d\lambda / \int_{200}^{2400} \varphi_{sol}(\lambda)\, d\lambda \text{- - - - - - - - (2)}$$

$$Tlum = \int_{380}^{800} \varphi_{lum}(\lambda) \cdot T(\lambda)\, d\lambda / \int_{380}^{800} \varphi_{lum}(\lambda)\, d\lambda \text{- - - - - - - - (3)}$$

The solar modulation was determined by the following formula: here the φ_{sol} (λ) is the solar irradiance spectrum distribution for AM 1.5 (corresponding to the sun standing 37º above the horizon with 1.5 atmosphere thickness and the presence of a solar zenith angle of 48.2º); $\varphi_{lum}(\lambda)$ is the standard luminous efficiency function of photopic vision for the wavelength of 380–800 nm[20]. T(λ) and R(λ) are the transmittance spectrum and reflectance spectrum. XRD patterns of CWO was collected by Rigaku SmartLab 9kW-advance using Theta/2 Theta mode, while other XRD patterns were collected by Rigaku SmartLab 9kW across the range of 20-80° with step size of 0.02° and scan rate of 10°/min under the 2 Theta mode. The glancing angle was set to 2°. The cone calorimeter (cone) test was performed on an apparatus of Fire Testing Technology according to ISO 5660. The samples of 100 × 100 × 3 mm^3 were burnt under an external heat flow of 35 kW/m^2. The vertical burning test was carried out on a laboratory assembled UL 94 vertical flame chamber according to ASTM D3801 with sample sizes of 130 × 13 × 3.2 mm^3. Thermogravimetry analysis (TGA) was obtained from PerkinElmer TGA 4000 System. 1-5 mg of the sample was heated from 25°C to 800 °C with the heating rate of 10 °C /min under the air flow of 50 mL/min. The thermal conductivity was obtained from a thermal conductivity meter equipped with a Hot Disk Kapton sensor, at a power of 200 mW and measuring time of 40s.

Solar blocking test

The solar blocking capacity (i.e., how much solar irradiation is transmitted) was simply evaluated by detecting the solar intensity behind the target sample at constant irradiance and at both ambient temperature and humidity. The center of solar light, solar intensity detector, and the center of the sample lie on the same straight line parallel to the table. Meanwhile, the lamp-sample and sample-detector distance were 15cm and 30 cm, respectively. For the blank sample, the sample holder was removed, allowing the light reading directly on the detector. Then the detected solar intensity was recorded after stabilization. The whole set was shown in Fig. S2.

Heat shielding simulation

The heat-shielding performance of normal glass, FRTW, and FRTW@$CWO_{0.75}$ were conducted using a custom heat shielding test configuration. A box made of expanded polypropylene (EPP) with the size of 340mm x 220mm x180 mm (wall thickness ~20 mm), the whole setup is shown in Fig S3). The FRTW, normal glass, and FRTW@$CWO_{0.75}$ (100 mm × 100 mm) were fixed on the top of the box. The light center and the center of the window lie on a straight line parallel to the table. The distance between the light center and the window center was set to 45 cm to ensure the solar intensity received at the window location is around 1000 W/m^2. A PT 100 temperature sensor was fixed at the bottom surface of the box, while another sensor was put in the box to monitor the indoor air temperature. The temperature data was exported by a MT21111-M2101 module (Smacq). The irradiation exposure was maintained for 15 mins, and then the bottom surface and indoor air were allowed to cool down to original temperature. Both the heating and cooling process were recorded. The environment temperature for the whole test was around 24 ^oC.

Energy saving simulation

The energy consumption simulation was conducted on *Energy Plus V22-2*, where a medium office prototype building model, as defined by the US Department of Energy, was used (Fig S4)[21]. The façade of the model and HVAC parameters are presented in Table S1. The building has a total area of 4982.19 m^2 with a 33% window to wall ratio. The glazing system has a total window area of 652.83 m^2. The optical properties of FRTW@$CWO_{0.75}$ and normal glass are shown in Table 2 (parameters of normal glass is cited from Wang's report[22]). Three typical cities (Hong Kong, Singapore, and Shanghai) were selected for the simulation. The building energy saving performance values are obtained by comparing the annual and monthly heating/cooling energy consumption between the different window materials.

Result and discussion

Structure and morphology

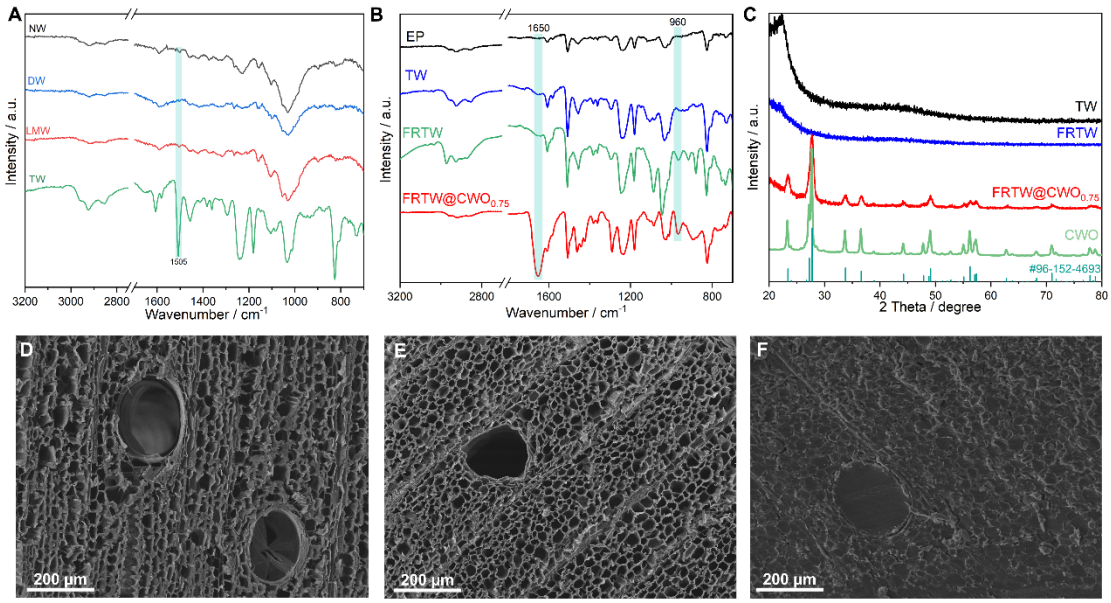

Figure. 1 (A) FTIR spectra of natural wood, delignified wood, lignin-modified wood, and transparent wood. (B) FTIR spectra of EP, TW, FRTW, and FRTW@$CWO_{0.75}$. *(C) XRD patterns of CWO, TW, FRTW, and* FRTW@$CWO_{0.75}$. *(D-F) Cross-sectional SEM images of natural wood (D), LMW (E), and FRTW (F).*

TW substrates used here were prepared from decoloring process followed by epoxy impregnation. The decoloring process was prepared by lignin modification route[19]. The FTIR spectra of natural wood (NW), delignified wood (DW), lignin-modified wood (LMW) and TW are shown in Fig.1A. The presence of the characteristic lignin peak (1507 cm^{-1}) in NW and LMW indicates the preservation of the lignin skeleton [23]. The FTIR spectra in Figure 1B show the comparison between pure epoxy (EP), TW, flame-retardant TW (FRTW), and FRTW@$CWO_{0.75}$. The presence of the peak at 960 cm^{-1} (P-O-C) indicates the inclusion of BPDP in the TW matrix [24]. While the peak at 1650 cm^{-1} is ascribed to the vibration of amide group in PVP. Although the characteristic peaks of CWO are not clearly visible in the FTIR spectra, the XRD pattern in Fig. 1C confirms its presence (#96-152-4693). The SEM image of CWO in Fig S5 displays particle sizes of approximately 50 nm. The cross-sectional SEM images of NW (Fig. 1D) and LMW (Fig. 1E) suggest that the highly aligned microchannels were well reserved after lignin modification, providing the space for subsequent polymer impregnation. As shown in Fig. 1F, the microchannels were fully impregnated with epoxy, showing no gaps between polymer and wood scaffold even after the incorporation of BPDP. This suggests that the flame retardant has remarkable compatibility with the epoxy matrix.

Optical properties and heat shielding performance

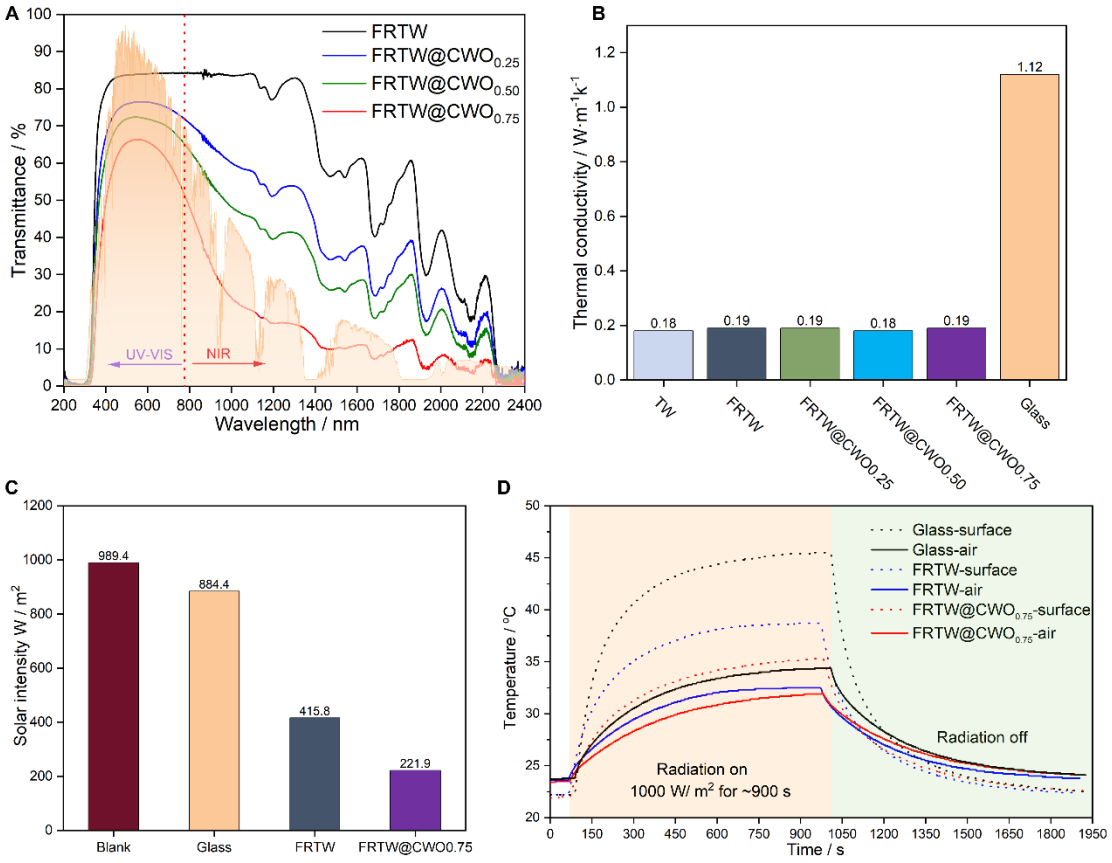

Figure. 2 (A) The transmittance of FRTW and FRTW@CWO in the solar spectrum. (B) The thermal conductivity of normal glass, TW, FRTW, and FRTW@CWO. (C) The detected solar intensity behind each sample at the distance of 45 cm. (D) The air temperature (T_a) inside of the box and the temperature at the bottom surface (T_s) during the irradiation on process and natural cooling process.

As shown in Fig S6, the visible transmittance of FRTW exhibited a slight decrease compared to the original TW. This suggests that BPDP has minimal impact on the optical properties of TW. The optical transmittance of RFTW and FRTW@CWO, crossing the UV-Vis-Near Infrared (200-2400 nm) are presented in Fig. 2A. A detail comparison in terms of transmission for FRTW and FRTW@CWO was provided in Table 1. FRTW allowed UV-VIS-NIR to pass through, leading to an increase of indoor temperature. While the total transmission was decreased with the increase of CWO concentration of the coating solution. The transmission in the NIR range for FRTW was 67.87%, while it decreased to 22.11% for FRTW@$CWO_{0.75}$, representing a reduction of 67.23%. FRTW@$CWO_{0.75}$ exhibited the lowest NIR transmittance (~47.20%) is probably due to the high absorption of $Cs_{0.33}WO_3$ in the NIR range [25]. This suggests that FRTW@$CWO_{0.75}$ may exhibit excellent heat-shielding performance for window applications, leading to significant energy savings. It is worth noting that both FRTW and coated FRTWs demonstrated low (7.05% to 16.04%) UV transmission, which is beneficial for prolonging the service life of indoor items such as furniture [26]. Additionally, FRTW@$CWO_{0.75}$ shows a transmittance (60.15%) in the visible range,

which is totally acceptable for window applications. The photograph of FRTW and FRTW@$CWO_{0.75}$ with the size of 10 cm × 10 cm are shown in Fig. S7. The symbols underneath of FRTW and FRTW@$CWO_{0.75}$ can be seen clearly, suggesting their considerable visual transmittance.

Table 1. Transmittance in different wavebands

Sample	UV / %	VIS / %	NIR / %
FRTW	16.04	83.39	67.87
FRTW@$CWO_{0.25}$	10.94	74.15	46.22
FRTW@$CWO_{0.50}$	9.88	69.25	36.73
FRTW@$CWO_{0.75}$	7.05	60.15	22.11

Thermal conductivity is another critical parameter for energy-saving performance. The thermal conductivity of glass, TW and FRTW@CWO are shown in Fig. 2B. Glass shows the highest thermal conductivity (~1.12 $W \cdot m^{-1}k^{-1}$), which is approximately six times higher than that of TW (~ 0.18 $W \cdot m^{-1}k^{-1}$), indicating the poor thermal insulating capacity of traditional glasses. This is one of the primary reasons why glasses are considered the most energy-inefficient part of a building envelope [27]. FRTW@$CWO_{0.75}$ exhibits a close thermal conductivity (~ 0.19 $W \cdot m^{-1}k^{-1}$) to that of TW (~ 0.18 $W \cdot m^{-1}k^{-1}$), suggesting that the CWO coating has minimal impact on thermal conductivity, and far superior to that of conventional glass substrates. The slight fluctuations in thermal conductivity are likely due to acceptable machine errors.

To assess the solar blocking performance, a simple solar blocking test was conducted using a setup shown in Fig S2. The solar irradiation intensity was measured by a TES 1333R solar meter. As depicted in Fig. 2C, the blank sample had a solar intensity of approximately 989.4 W/m² at a lamp-solar meter distance of 45 cm. Glass exhibited limited solar-blocking capacity, resulting in a solar intensity of 884.4 W/m². FRTW demonstrated a significantly lower detected solar intensity of 415.8 W/m² due to its inherent light scattering effect. FRTW@$CWO_{0.75}$ exhibited a solar intensity of 221.9 W/m², indicating a reduction of 46.63%, which aligns with the calculated reduction based on the spectra.

To further investigate the heat-shielding performance of TW composites, a field test was conducted with a setup displayed in Figure S3. Glasses, FRTW, and FRTW@$CWO_{0.75}$ were fixed as windows on the top of an EPP box. Two PT 100 temperature sensors were used to continuously monitored the air temperature (T_a) inside the box and the temperature at the bottom surface (T_s) of the box (Fig 2D). A PLS-SXE300D xenon lamp was used to simulate solar irradiation, ensuring that the light spot was centered on each sample. The distance between the window and lamp was fixed at 45 cm to achieve a detected solar irradiation power of around 1000 W/m². After approximately 15 minutes of solar irradiation, the T_s of glass reached 45.5°C, while those of FRTW and FRTW@$CWO_{0.75}$ decreased to 38.7°C and 35.3°C, respectively. In terms of indoor air temperature (T_a), glass increased to 34.2°C after 15 minutes of solar irradiation. In the case of FRTW, T_a increased to 32.5°C, which is

1.7°C lower than that of glass. FRTW@$CWO_{0.75}$ exhibited the lowest T_a of 31.9°C after 15 minutes of irradiation, representing a reduction of 2.3°C compared to normal glass. The desired reductions in Ta and Ts demonstrate the remarkable heat-shielding performance of FRTW@$CWO_{0.75}$. These results suggest that FRTW@$CWO_{0.75}$ could be a promising candidate for window applications, particularly in hot areas and climates.

Energy Consumption Simulation

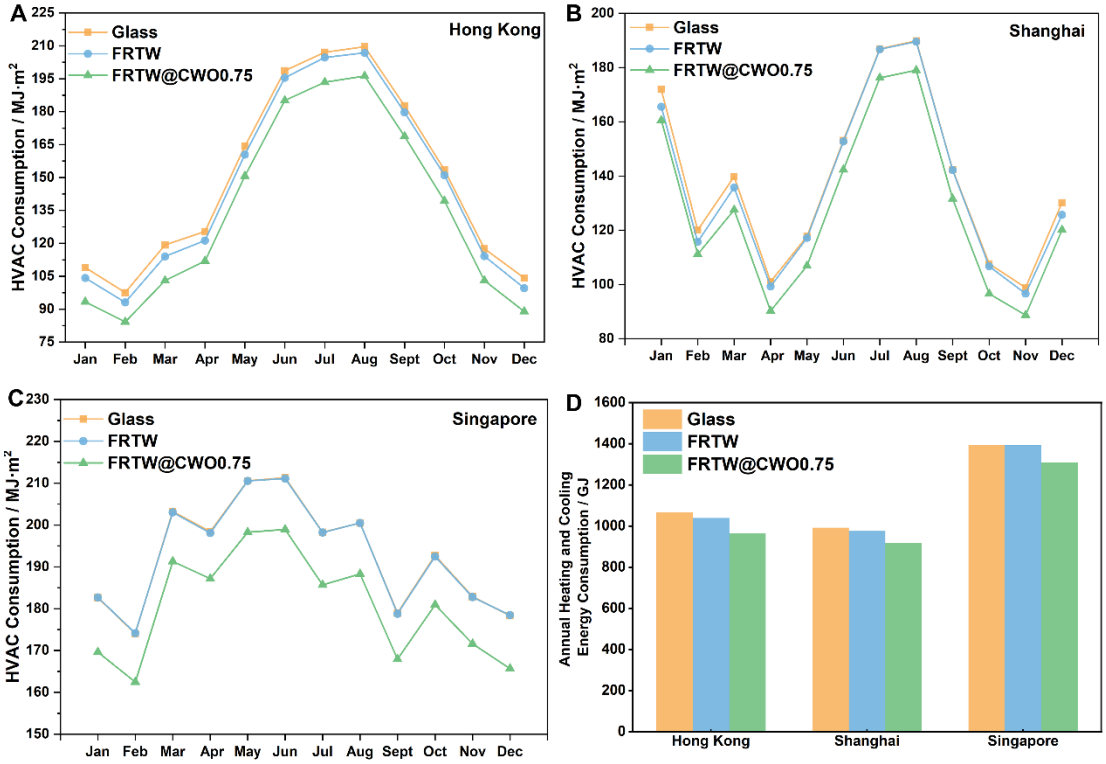

Figure. 3 (A-C) Simulated monthly energy consumption comparisons between glass, FRTW and RTW@$CWO_{0.75}$ in Hong Kong (Zone 2A), Shanghai (Zone 3A), and Singapore (Zone 0A). (D) Annual heating and cooling energy consumption of glass, TW and FRTW in Hong Kong, Shanghai, and Singapore.

To quantitatively demonstrate the energy saving potential of RTW@$CWO_{0.75}$, energy saving simulation was conducted using EnergyPlus (V22.2). Three typical cities (Hong Kong (Zone 2A), Singapore *(Zone 0A)*, and Shanghai (Zone 3A)) were selected for the simulation. Energy saving potential of RTW@$CWO_{0.75}$ was compared with normal glass and FRTW. The monthly energy consumption of RTW@$CWO_{0.75}$, FRTW and normal glass were shown in the Fig. 3A-C. FRTW@$CWO_{0.75}$ exhibited the lowest monthly HVAC consumption among three selected cities. While FRTW showed almost the same monthly HVAC consumption as the normal glass due to is high solar transmission. The annual heating and cooling energy consumption was presented in Fig. 3D. The RTW@$CWO_{0.75}$ showed an energy saving rate of 9.6 %, 7.7%, and 6.2 % in Hong Kong, Shanghai, and Singapore, respectively. Overall, FRTW@$CWO_{0.75}$ demonstrated the lowest annual heating and cooling energy consumption, highlighting its potential for significant energy savings in buildings.

Flame retardancy and thermal properties

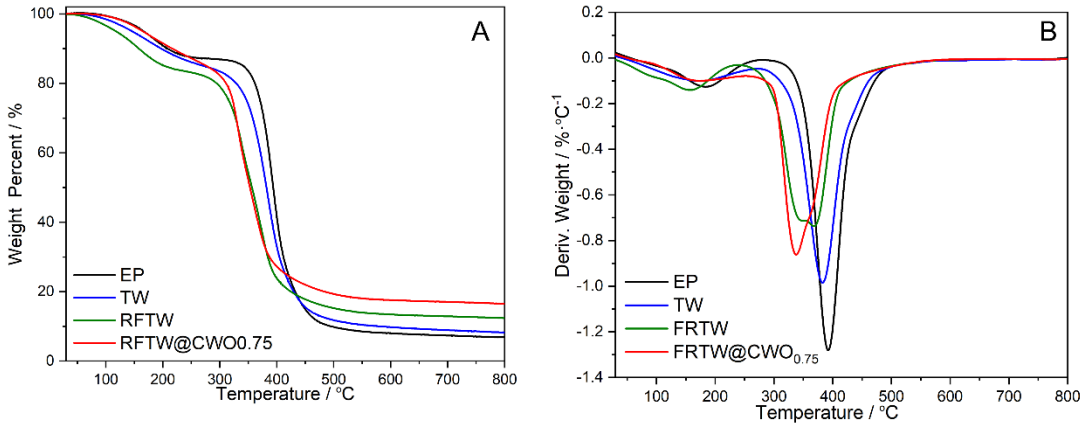

Figure. 4 TG(A) and DTG(B) curves of EP, TW, FRTW and FRTW@$CWO_{0.75}$ *under nitrogen atmospheres.*

Despite the promising energy-saving properties, the fire safety of TW composites is usually considerably lower than traditional glasses, which are completely nonflammable. To address the fire safety concerns associated with TW composites, BPDP was incorporated into the TW matrix to enhance its fire resistance, thereby making it more suitable for real-world applications. The thermal stability of EP, TW, FRTW and FRTW@$CWO_{0.75}$ are measured by TGA under nitrogen flow, TG and DTG curves are presented in Fig. 4. The decomposition temperature (T_d, temperature at 5% mass loss), the temperature at maximum weight loss rate (T_{max}) and the char yield (CY) at 700 °C, are listed in the Table 2.

Table 2 Thermal decomposition data for EP, TW and TW composites.

Sample	[a]T_d / °C	[b]T_{max} / °C	[c]CY / wt %
EP	166.3	393.0	7.3
TW	146.3	383.2	8.9
FRTW	117.0	368.8	12.9
FRTW@$CWO_{0.75}$	165.0	338.2	17.1

a Temperature at 5% of weight loss. b Temperature at maximum decomposition rate. c Residue yield at 700 °C.

Two distinct stages of decomposition can be readily observed in the TG and DTG curves. The decomposition temperature (T_d) of the epoxy (EP) is noticeably lower (~166.3 °C) compared to previous findings[28, 29], which can be attributed to the specific epoxy composition employed in this study. The T_d of TW is lower than that of EP due to the presence of wood scaffold. While the T_d was decreased to 117.0 °C upon the incorporation of BPDP, indicating an acceleration of the decomposition process at the initial stage[30, 31]. Such accelerating effect can be ascribed to catalytic effect of the phosphorus-based acids generated by the phosphorus-containing flame retardant.

Notably, the T_d of FRTW@$CWO_{0.75}$ increased to 165.0 °C due to the presence of the CWO coating. Similarly, the T_{max} of FRTW decreased in comparison to pure EP, indicating that the degradation products of the flame retardant might facilitate the earlier degradation of epoxy chains. The DTG curve demonstrates a significant reduction in the maximum decomposition rate after the incorporation of BPDP, suggesting that despite the promotion of early degradation, BPDP may inhibit the overall decomposition rate. Additionally, the char yield (CY) of FRTW exhibited a substantial increase (from 7.3% to 12.9%), indicating the carbonization effect induced by BPDP. Interestingly, this value further increased to 17.1% following CWO coating, highlighting the catalytic carbonization effect exhibited during the decomposition process, akin to other inorganic substances[32-34]. The promoted carbonization effect may contribute to the formation of protective char layers during combustion.

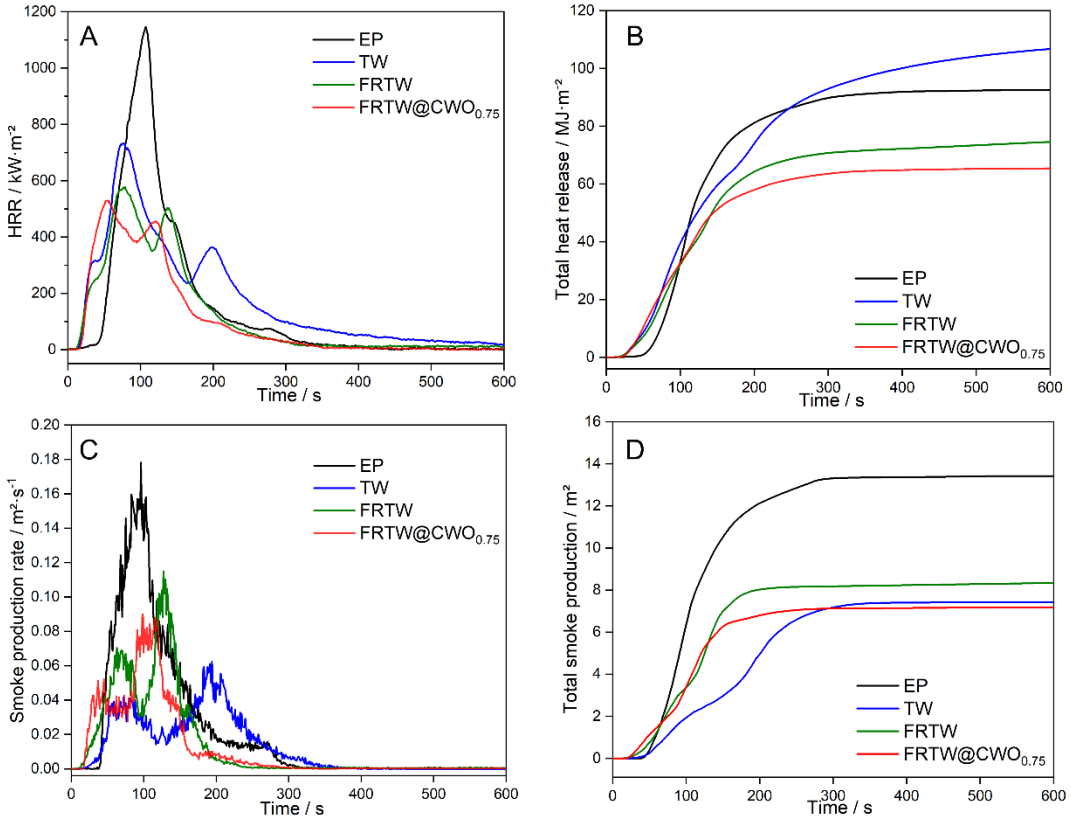

Figure. 5 HRR (A), THR (B), SPR(C) and TSR (D) curves of EP, TW, FRTW, and FRTW@$CWO_{0.75}$.

To further investigate the fire safety of TW composites, Cone and vertical burning test was performed. HRR (heat release rate), THR (total heat release), SPR (smoke production rate), TSP (total smoke production) curves and related combustion parameters are presented in the Fig. 5 and Table 3, respectively.

Table 3 Combustion parameters of TW composites

Sample	TTI / s	HRR/ $kW \cdot m^{-2}$	THR/ $MJ \cdot m^{-2}$	SPR/ $m^2 \cdot s^{-1}$	TSP/ m^2	COY /$kg \cdot kg^{-1}$	UL-94
EP	18	1146.23	93.58	0.18	13.57	0.11	\[a]
TW	13	732.64	109.75	0.06	7.44	0.15	\[a]
FRTW	9	577.43	76.54	0.12	8.43	0.15	V1(7± 1[b], 8±1[c])
FRTW@$CWO_{0.75}$	14	529.55	65.93	0.09	7.19	0.22	V1(7± 1[b], 7±1[c])

TTI: time to ignition; HRR: peak heat release rate; THR: total heat release; SPR: peak smoke production rate; TSP: total smoke production; COY: average carbon monoxide yield; [a] Completely burn out after the first ignition, no rating; [b] The average self-extinguish time after the first 10 s ignition; [c] The average self-extinguish time after the second 10 s ignition.

The inclusion of BPDP in the system leads to a decreased time to ignition (TTI), indicating an accelerated degradation of epoxy chains, as indicated by the TG results. Interestingly, the TTI of FRTW@$CWO_{0.75}$ (14 s) was significantly higher than that of FRTW (9 s), possibly due to the heat irradiation shielding effect of the CWO coating. TW shows a HRR value of 732.64 $kW \cdot m^{-2}$, whereas HRR of FRTW was decreased significantly (~21.2% of reduction, 577.43 $kW \cdot m^{-2}$) due to the presence of BPDP. The decreased HRR may results from the promoted char formation by the decomposition products of BPDP, as well as the phosphorous free radicals contained in the pyrolysis products. The HRR of FRTW@$CWO_{0.75}$ was further decreased to 529.55 $kW \cdot m^{-2}$ (a reduction of 27.7 % compared to the original TW) due to the catalytic carbonization effect of CWO, forming more protective char layers during the combustion. Compared to the TW, the incorporation of BPDP brings 30.3 % (from 109.75 to 76.54 $MJ \cdot m^{-2}$) reduction of THR, indicating the remarkable flame-retardant efficiency. After CWO coating, this value was further decreased to 65.93 $MJ \cdot m^{-2}$ due to the catalytic carbonization effect of CWO. TW exhibits a SPR of 0.06 $m^2 \cdot s^{-1}$, while this value fallen to 0.12 $m^2 \cdot s^{-1}$ after incorporating BPDP into TW. The enhanced SPR is also observed for other phosphorous-containing flame retardants[35]. FRTW@$CWO_{0.75}$ shows a TSP of 7.19 m^2, which is slightly higher than that of FRTW (8.43 m^2), revealing the smoke suppression effect of CWO particles. The COY was increased after the incorporation of BPDP due to more incomplete combustion, which resulted from the insufficient oxygen supply (caused by the barrier effect of the protective char layers). The pure EP and TW are burn out completely after the first ignition. However, with the addition of BPDP (10 wt%), FRTW and FRTW@$CWO_{0.75}$ can reach the rating of V1. This may indicate that though the CWO coating have synergetic effect on combustion behaviors from a micro perspective combustion (e.g., reduced HRR and SPR compared to FRTW), it may have limited impact on macro combustion behaviors (i.e., unchanged UL-94 rating compared to FRTW). Overall, both the cone results and the vertical burning test indicate the improved fire safety.

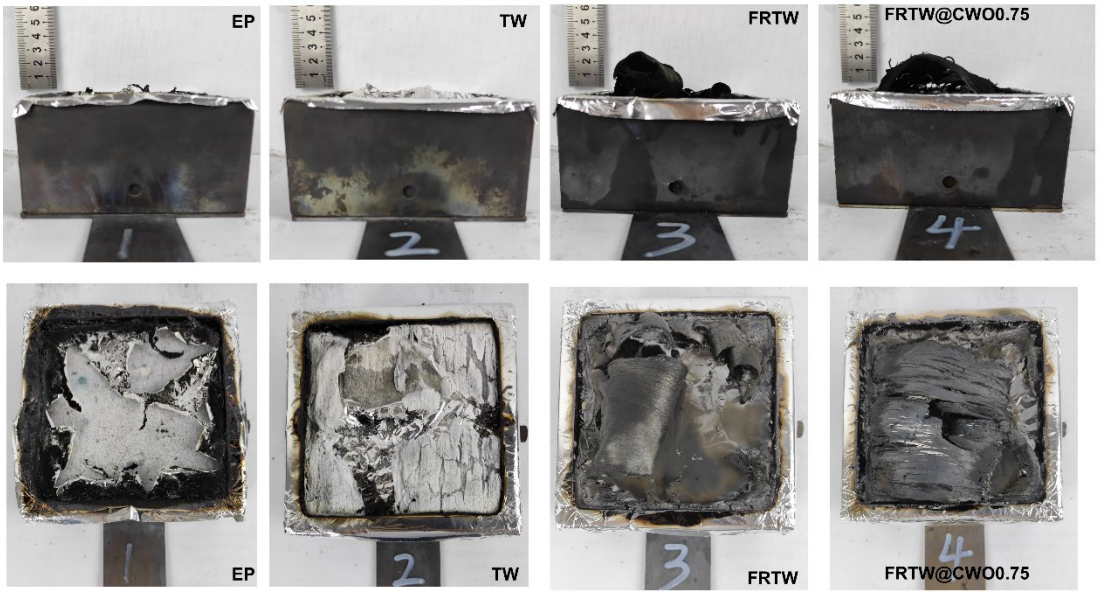

Figure.6 Side (up) and top (bottom) photographic view of char residues after cone test.

Fig. 6 displays the digital photos obtained after the cone test, revealing the outcomes of the different samples. It is evident that EP and TW were completely consumed with very limited rigid char layers. In contrast, both FRTW and FRTW@$CWO_{0.75}$ exhibited a notable intumescent effect, characterized by the formation of continuous protective char layers. These findings collectively indicate that the inclusion of BPDP contributes to enhanced fire safety.

Conclusion

This study presents the first reported preparation of a combined heat-shielding and flame-retardant transparent wood (TW) using a post-functionalization approach. The surface of TW was successfully coated with $Cs_{0.33}WO_3$ to block NIR irradiation, and a liquid and transparent flame retardant (BPDP) was introduced to enhance fire safety. The FRTW and FRTW@$CWO_{0.75}$ can reach a UL-94 rating of V1. Moreover, compared to the original TW, FRTW@$CWO_{0.75}$ demonstrated improved fire safety due to the incorporation of BPDP, resulting in a 27.7% reduction in heat release rate (HRR). The two components also seemingly had a synergic effect in improving the relevant flame-retardant characteristics; both the ignition time and the HRR were increased with the $Cs_{0.33}WO_3$ addition, as compared to BPDP performance alone. With the combination of $Cs_{0.33}WO_3$ coating and BPDP, the char yield (CY) of heat-shielding TW was increased from 7.3% to 17.1%. FRTW@$CWO_{0.75}$ exhibited considerable solar-blocking capacity and thermal insulating performance, enabling it to be a promising candidate for energy saving applications. FRTW@$CWO_{0.75}$ exhibited a favorable visible transmittance of 60.15% for window applications, while allowing only 22.11% of NIR irradiation to pass through. Field tests confirmed that FRTW@$CWO_{0.75}$ effectively reduced indoor temperatures by 10.2°C compared to glass. Energy simulations also indicated that FRTW@$CWO_{0.75}$ could achieve energy savings of 9.6%, 7.7%, and 6.2% in annual heating and cooling energy consumption for Hong Kong, Shanghai, and Singapore, respectively. With its desirable combination of synergistic heat-shielding performance and enhanced fire safety features, FRTW@$CWO_{0.75}$ emerges as a highly promising candidate for energy-efficient windows and transparent structures.

Acknowledgements: All authors would like to thank the Hong Kong Environment and Conservation Fund (Grant code: ECF 107/2020, P0034081), and PolyU (1-BBCB) for funding.

Consent for publication: All authors agree to the submission and publication of article materials.

Conflicts of Interest: There are no known conflicts to declare.

Reference

[1] E. Cuce, S.B. Riffat, A state-of-the-art review on innovative glazing technologies, Renewable and Sustainable Energy Reviews 41 (2015) 695-714.

[2] H. Ye, X. Meng, L. Long, B. Xu, The route to a perfect window, Renewable Energy 55 (2013) 448-455.

[3] D.D. Furszyfer Del Rio, B.K. Sovacool, A.M. Foley, S. Griffiths, M. Bazilian, J. Kim, D. Rooney, Decarbonizing the glass industry: A critical and systematic review of developments, sociotechnical systems and policy options, Renewable and Sustainable Energy Reviews 155 (2022) 111885.

[4] M. Brzezicki, The Influence of Reflected Solar Glare Caused by the Glass Cladding of a Building: Application of Caustic Curve Analysis, Computer-Aided Civil and Infrastructure Engineering 27(5) (2012) 347-357.

[5] X. Hu, Y. Zhang, J. Zhang, H. Yang, F. Wang, F. Bin, N. Noor, Sonochemically-coated transparent wood with ZnO: Passive radiative cooling materials for energy saving applications, Renewable Energy 193 (2022) 398-406.

[6] S.T. Lazar, T.J. Kolibaba, J.C. Grunlan, Flame-retardant surface treatments, Nature Reviews Materials 5(4) (2020) 259-275.

[7] Z. Li, W. Wei, W. Wang, Y. Sun, S. Wang, Y. Lin, C. Huang, Y. Wu, S. Deng, A method for sizing air source heat pump considering the joint effect of outdoor air temperature and relative humidity, Journal of Building Engineering 65 (2023) 105815.

[8] Y. Li, Q. Fu, X. Yang, L. Berglund, Transparent wood for functional and structural applications, Philosophical Transactions of the Royal Society A: Mathematical, Physical and Engineering Sciences 376(2112) (2017) 20170182.

[9] M. Zhu, J. Song, T. Li, A. Gong, Y. Wang, J. Dai, Y. Yao, W. Luo, D. Henderson, L. Hu, Highly Anisotropic, Highly Transparent Wood Composites, Advanced Materials 28(26) (2016) 5181-5187.

[10] Y. Li, Q. Fu, S. Yu, M. Yan, L. Berglund, Optically Transparent Wood from a Nanoporous Cellulosic Template: Combining Functional and Structural Performance, Biomacromolecules 17(4) (2016) 1358-1364.

[11] T. Chu, Y. Gao, L. Yi, C. Fan, L. Yan, C. Ding, C. Liu, Q. Huang, Z. Wang, Highly fire-retardant optical wood enabled by transparent fireproof coatings, Advanced Composites and Hybrid Materials 5(3) (2022) 1821-1829.

[12] L. Chen, Z. Xu, F. Wang, G. Duan, W. Xu, G. Zhang, H. Yang, J. Liu, S. Jiang, A flame-retardant and transparent wood/polyimide composite with excellent mechanical strength, Composites Communications 20 (2020) 100355.

[13] C. Fan, Y. Gao, Y. Li, L. Yan, Y. Zhuang, Y. Zhang, Z. Wang, A flame-retardant and optically transparent wood composite, Journal of Applied Polymer Science 139(39) (2022) e52945.

[14] D. Yoon, H.T. Jung, G. Kwon, Y. Yoon, M. Lee, I. Bae, B.J. Joo, M. Kim, S.A. Lee, J. Lee, Y. Lee, E. Cho, K. Shin, B.J. Sung, Dynamics and Mechanism of Flame Retardants in Polymer Matrixes: Experiment and Simulation, The Journal of Physical Chemistry B 117(28) (2013) 8571-8578.

[15] X. Hu, R. Yu, F. Wang, Z. Liu, H. Yang, C. Chen, Y. Li, N. Noor, B. Fei, Fabrication, Functionalities and Applications of Transparent Wood: A Review, Advanced Functional Materials n/a(n/a) (2023) 2303278.

[16] Z. Yu, Y. Yao, J. Yao, L. Zhang, Z. Chen, Y. Gao, H. Luo, Transparent wood containing CsxWO3 nanoparticles for heat-shielding window applications, Journal of Materials Chemistry A 5(13) (2017)

6019-6024.
[17] T. Wu, Y. Xu, Z. Cui, H. Li, K. Wang, L. Kang, Y. Cai, J. Li, D. Tian, Efficient Heat Shielding and Ultraviolet Isolating Transparent Wood via In Situ Generation of TiO2 Nanoparticles, ACS Sustainable Chemistry & Engineering 10(47) (2022) 15380-15388.
[18] Z. Qiu, Z. Xiao, L. Gao, J. Li, H. Wang, Y. Wang, Y. Xie, Transparent wood bearing a shielding effect to infrared heat and ultraviolet via incorporation of modified antimony-doped tin oxide nanoparticles, Composites Science and Technology 172 (2019) 43-48.
[19] Y. Li, Q. Fu, R. Rojas, M. Yan, M. Lawoko, L. Berglund, Lignin-Retaining Transparent Wood, ChemSusChem 10(17) (2017) 3445-3451.
[20] G. Wyszecki, W.S. Stiles, Color science: concepts and methods, quantitative data and formulae, John wiley & sons2000.
[21] M. Deru, K. Field, D. Studer, K. Benne, B. Griffith, P. Torcellini, U.S. Department of Energy Commercial Reference Building Models of the National Building Stock. (2011).
[22] S. Wang, T. Jiang, Y. Meng, R. Yang, G. Tan, Y. Long, Scalable thermochromic smart windows with passive radiative cooling regulation, Science 374(6574) (2021) 1501-1504.
[23] M. Traoré, J. Kaal, A. Martínez Cortizas, Application of FTIR spectroscopy to the characterization of archeological wood, Spectrochimica Acta Part A: Molecular and Biomolecular Spectroscopy 153 (2016) 63-70.
[24] J. Feng, J. Hao, J. Du, R. Yang, Using TGA/FTIR TGA/MS and cone calorimetry to understand thermal degradation and flame retardancy mechanism of polycarbonate filled with solid bisphenol A bis(diphenyl phosphate) and montmorillonite, Polymer Degradation and Stability 97(4) (2012) 605-614.
[25] J. Liu, J. Luo, F. Shi, S. Liu, C. Fan, Q. Xu, G. Shao, Synthesis and characterization of F-doped Cs0.33WO3−xFx particles with improved near infrared shielding ability, Journal of Solid State Chemistry 221 (2015) 255-262.
[26] A.L. Andrady, A.M. Heikkilä, K.K. Pandey, L.S. Bruckman, C.C. White, M. Zhu, L. Zhu, Effects of UV radiation on natural and synthetic materials, Photochemical & Photobiological Sciences (2023).
[27] F. Hu, L. An, C. Li, J. Liu, G. Ma, Y. Hu, Y. Huang, Y. Liu, T. Thundat, S. Ren, Transparent and Flexible Thermal Insulation Window Material, Cell Reports Physical Science 1(8) (2020) 100140.
[28] X. Hu, H. Yang, Y. Jiang, H. He, H. Liu, H. Huang, C. Wan, Facile synthesis of a novel transparent hyperbranched phosphorous/nitrogen-containing flame retardant and its application in reducing the fire hazard of epoxy resin, Journal of Hazardous Materials 379 (2019) 120793.
[29] X. Hu, M. Li, J. Yang, F. Liu, H. Huang, H. Pan, H. Yang, In situ fabrication of melamine hydroxy ethylidene diphosphonate wrapped montmorillonite for reducing the fire hazards of epoxy resin, Applied Clay Science 201 (2021) 105934.
[30] H. Yang, L. Song, Q. Tai, X. Wang, B. Yu, Y. Yuan, Y. Hu, R.K.K. Yuen, Comparative study on the flame retarded efficiency of melamine phosphate, melamine phosphite and melamine hypophosphite on poly(butylene succinate) composites, Polymer Degradation and Stability 105 (2014) 248-256.
[31] X. Feng, H. Yang, Boosting flame retardancy of thermoplastic polyurethane: Synergistic effect of nickel phosphide nanoparticles and molybdenum disulfide nanosheets, Journal of Vinyl and Additive Technology 29(3) (2023) 522-533.
[32] J. Yang, A. Zhang, Y. Chen, L. Wang, M. Li, H. Yang, Y. Hou, Surface modification of core–shell structured ZIF-67@Cobalt coordination compound to improve the fire safety of biomass aerogel insulation materials, Chemical Engineering Journal 430 (2022) 132809.
[33] B. Yu, B. Tawiah, L.-Q. Wang, A.C. Yin Yuen, Z.-C. Zhang, L.-L. Shen, B. Lin, B. Fei, W. Yang, A.

Li, S.-E. Zhu, E.-Z. Hu, H.-D. Lu, G.H. Yeoh, Interface decoration of exfoliated MXene ultra-thin nanosheets for fire and smoke suppressions of thermoplastic polyurethane elastomer, Journal of Hazardous Materials 374 (2019) 110-119.
[34] F. Liang, Y. Xu, S. Chen, Y. Zhu, Y. Huang, B. Fei, W. Guo, Fabrication of Highly Efficient Flame-Retardant and Fluorine-Free Superhydrophobic Cotton Fabric by Constructing Multielement-Containing POSS@ZIF-67@PDMS Micro–Nano Hierarchical Coatings, ACS Applied Materials & Interfaces 14(50) (2022) 56027-56045.
[35] T. Mariappan, Y. Zhou, J. Hao, C.A. Wilkie, Influence of oxidation state of phosphorus on the thermal and flammability of polyurea and epoxy resin, European Polymer Journal 49(10) (2013) 3171-3180.